

We are IntechOpen, the world's leading publisher of Open Access books Built by scientists, for scientists

6,900

Open access books available

186,000

International authors and editors

200M

Downloads

Our authors are among the

154

Countries delivered to

TOP 1%

most cited scientists

12.2%

Contributors from top 500 universities



WEB OF SCIENCE™

Selection of our books indexed in the Book Citation Index
in Web of Science™ Core Collection (BKCI)

Interested in publishing with us?
Contact book.department@intechopen.com

Numbers displayed above are based on latest data collected.
For more information visit www.intechopen.com



Human-Robot Interface for end effectors

Marcin Kaczmarek

*Technical University, Institute of Automatic Control I-13
Poland*

1. Abstract.

This paper focuses on a comprehensive description of the artificial hand and its driving mechanisms. Static and dynamic parameters of the model are detailed. The kinematics of the hand and its application in visual control are presented. Each joint of the designed hand is driven by a pair of McKibben muscles. Due to their parameters – high overloading and stiffness control capabilities, they are very suitable for environment interaction. The chosen actuators - pneumatic muscles, are also a simplified substitute for human muscles. Modeling the work of the human hand can in this case be conducted in a limited range. On the other hand, these limitations simplify the vision analysis, which was adequately considered in the algorithms of image processing. When designing the software, it was attempted to use only that information, which is necessary to accomplish a given task and the interaction of the hand with the steered object. A cue acquired from a biosignal measuring system is the main signal initiating the gripping phase. All miopotentials are recorded by an active surface electrode. The paper presents the problems of artifacts in the measured signal and solutions which allow for reducing their level. It also shows a schematic of laboratory stand, which is used for electromiografy recording and controlling the finger banding process of the artificial hand. The paper ends with collected conclusions from the research projects conducted by our team and the future plans concerning improved replication of human movements and using a stereoscopic view in vision control.

2. Introduction

Evolution of robotic constructions can be observed all over the world. Robots replace human work in many areas. They work in environments that are harmful to humans and are used for tasks requiring precision of movements. To this purpose manipulators of a different kind are being built, starting from structures with a serial kinematical chain to ones with a parallel one which is more commonly used at the present. Unfortunately, these kinds of structures are designed only for one type of tasks. That is why humans try to “spy the nature” to get the inspiration for new, more versatile projects. As always, an unreachable construction goal is the imitation of a human being. Besides of locomotive functions this kind of robot should be able to manipulate in any environment where it is placed. Synthesis of manipulation and locomotion in an anthropomorphic construction is developed by the Honda corporation, where humanoid robots P3 and Asimo were created. Although their external shape is similar to human beings, they can only try to imitate the smoothness of

their natural equivalent. Human smooth gait is a complex process and cannot be replaced by any control algorithm. It is characterized by a dynamic phase which is unreachable by electrical motors. Another construction of anthropomorphic biped robot is proposed by a British company "Shadow". In their project they use artificial McKibben muscles for actuating robot joints. These muscles are characterized by variable stiffness (Feja K., Kaczmariski M., Riabcew P., 2005) which makes smooth and dynamic movement possible. Imperfection of this actuator is the nonlinear force characteristic, which makes control more complex in comparison to electric motors.

Another problem for humanoid robots is the manipulation of objects. To this purpose different kinds of grippers are created. Starting from a simple one with the basic types of grasps, to more complicated ones that provide adaptability to different forms of objects.

Created in the Institute of Automatic Control, the artificial hand is a simplified imitation of the human natural hand. Artificial muscles which were used for actuating the hand are also very simple compared to equivalent natural ones. This of course influences the modeling of movements, making them limited.

In most artificial grippers internal sensors of fingers' positions are used to control movements. Additional force sensors allow recognizing the pressure of fingers during contact with an object and providing grasp adaptation.

This chapter shows that also a vision system can be used to recognize the position of fingers and control the precision and force of grasping. The created artificial hand has no internal sensors, so control is achieved by only the information obtained from the vision system. Although there are no pressure sensors on the finger tips, this kind of control is able to provide precision and regulate the force of grasping which will be shown in the text. Limitations in the construction of the artificial hand allowed to introduce some simplifications into the vision control algorithm. In the further part of the text the focus will be given to the construction properties of the created artificial hand and pneumatic muscles, which are used for actuating the fingers and wrist joints. A mathematical analysis of the kinematic model of the hand and its adaption to vision control for analysis by specific trajectories will be presented. The strategies of grasping and photos presenting the results of the vision control application in an artificial hand control will also be described.

This chapter also presents the biopotential recordings for simple movement driving. For acquisition of the EMG signals a surface-active electrode was constructed. Its purpose was the preliminary preparation of measured signals. It was placed near the selected muscle groups to minimize the interferences. The collected signals were submitted to further processing and to digital acquisition. The created computer algorithm, basing on the myopotential signal, determines the effective (root mean square) value, which in the simplest form is dependant on the tension of the examined muscle. The computer program then controls the electro-valves, which set the appropriate pressure levels in the pneumatic muscles. The muscles actuate active joints in the artificial hand, causing the fingers to tighten. The presented interface for the control of various robotic constructions will be used in future projects in our laboratory.

3. Construction of the artificial hand

The view of an artificial hand is presented on Figure 1.

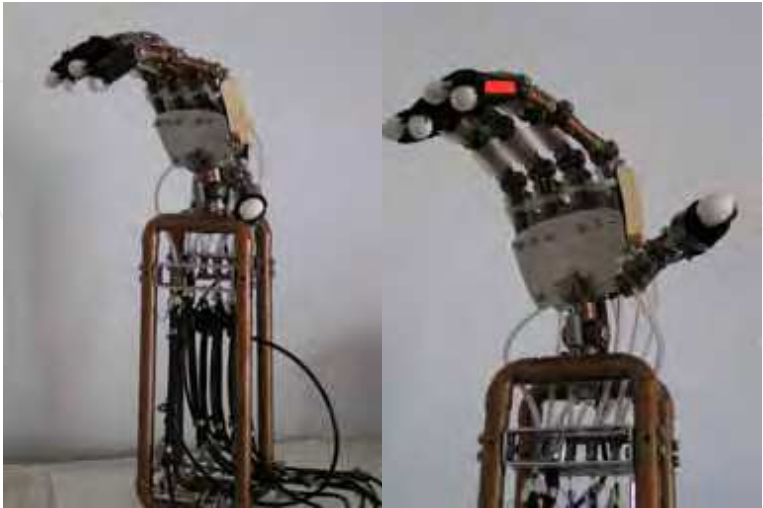


Figure 1. Real view of an artificial hand

The artificial hand can be divided into a number of segments. The biggest one is the structure of the forearm, which holds two layers of pneumatic muscles. The upper one contains two rows of actuators and they are linked in pairs. Each pair is connected to an active finger joint by the Kevlar tendons. Two muscles work in opposition to provide full banding and straightening of each finger. The thumb is actuated by only one pneumatic muscle, because its backward movement is provided by a spring and the gravitational force. The bottom layer contains only two actuators. One is responsible for rotating the hand in the wrist. This movement is similar to the pronation/supination. The second muscle provides the rotation of the thumb in the plane parallel to the surface of the palm. In both situations a spring element generates the force required for backward rotation. This force is proportional to extension of the spring and provides constant inclination of this value during the filling up of the muscle with compressed air. The force characteristic of an artificial muscle is linear in the initial range, so the rotation of the joint is proportion to the air pressure in the muscle.

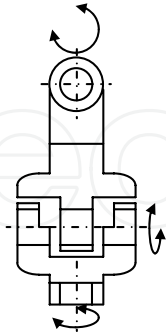


Figure 2. Wrist schematic

The second part of an artificial hand is the wrist. It consists of three independent rotary joints. They are placed near together and oriented in a way providing rotation around XYZ

axis of Cartesian coordinates. The real human wrist has only 2 DOF. The rotation (pronation-supination) in the human hand takes place in the forearm. This type of movement is implemented in the wrist of the artificial hand and increases its object manipulation capabilities. A schematic of the wrist is presented in Figure 2.

The last part of the designed construction is made up of the five fingers on an artificial palm. Every finger (except the thumb) contains three simple rotary joints with 1 DOF, while the thumb contains four. This allows the thumb tip for movements in two parallel planes. The total length of fully extended finger is 120mm. The presented artificial hand model allows fingers to bend completely, which is obtained by simultaneous rotation of all three rotary joints to the same angle. Thanks to this construction it was possible to use only one pair of actuators to drive the first active joint in the finger. Although this kind of solution causes limitations of number of DOF, it reduces the number of actuators required for movement generation.

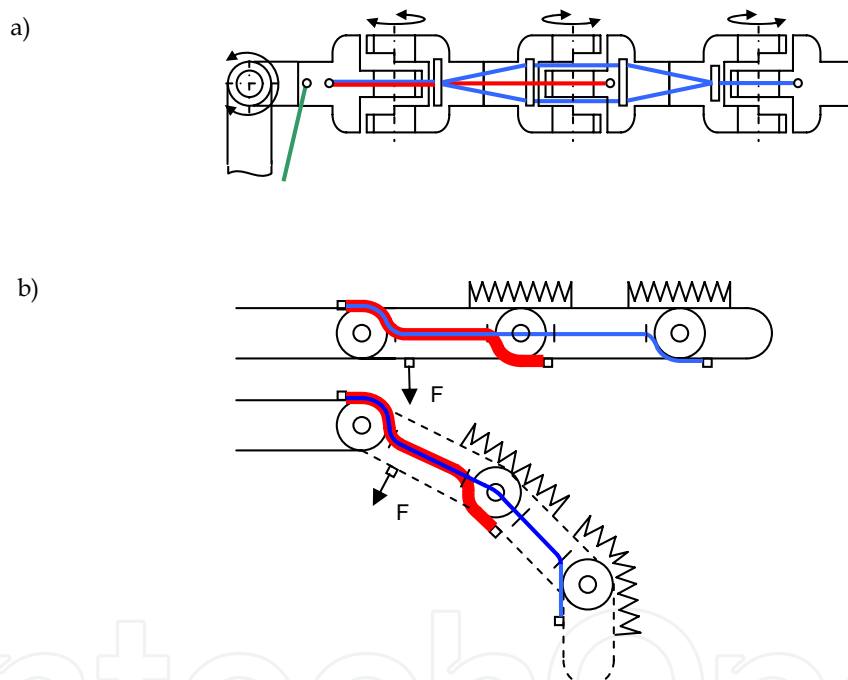


Figure 3. Arrangement of tendons in the fingers a) top view, b) side view

The picture in Fig.3. shows the arrangement of the Kevlar tendons in every finger. All wires being part of the mechanical coupling are attached to the top side of the palm. The other end of the wire is connected to the bottom side of the passive joint. When the active joint rotates, the length of the wire between attaching point and first slide increases while the length between the second end of the wire and the nearest slide decreases simultaneously. This provides the same angle of rotation in every joint of the finger. Every passive joint contains a spring element required for preventing spontaneous descending and providing linear relation of the compressed air pressure in the muscle.

4. System of the driveline

All actuators are connected to the active joints by the Nylon-Kevlar wire. The same kind of tendons are used to transfer the force from the active joints to the passive ones. Their undoubted advantage is a low friction coefficient and high tensile strength, that is the ratio of maximum braking power to the initial cross section field.

5. Characteristic data of the hand

The most important static and dynamic parameters of the created construction are presented below. It shows that the designed gripper with its size and movement possibilities is similar to a natural human limb.

5.1. Dimensions of the artificial hand

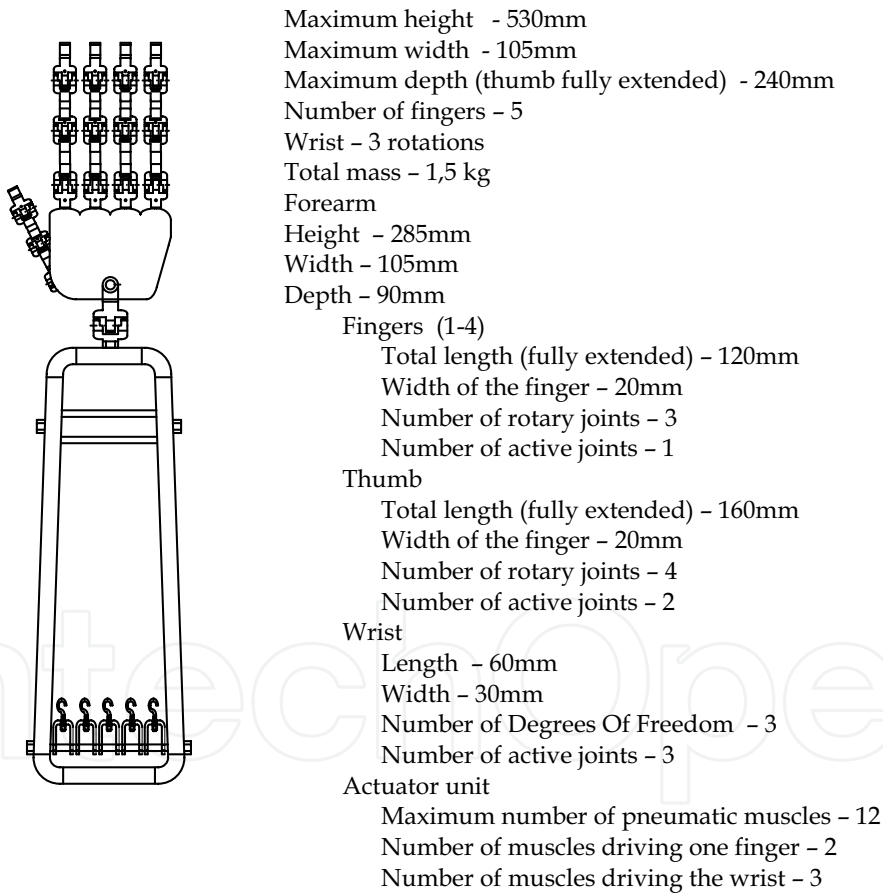


Figure 4. Schematic view of the designed hand

5.2. Dynamic specifications of the constructed hand

In order to calculate the parameters of the artificial hand, the maximum pressures of one finger in fully extended and folded states were measured. Also, a frequency of the bending-straightening cycle was calculated. All results are presented in the table below.

Maximum pressure of a finger fully bent	0,64 N
Maximum pressure of a straight finger (one opposing muscle per one finger)	0,78 N
Maximum pressure of a straight finger (two opposing muscles per one finger)	1,37 N
Maximum pressure of three fingers working simultaneously	1,91 N
Maximum frequency of the bending-straightening cycle	0,87Hz
Working frequency of the bending-straightening cycle	0,15Hz

Table 1. Dynamic parameters of the hand

1. Artificial McKibben Muscles

Pneumatic McKibben muscles were used for the first time in 1950 for testing of artificial limb replacements. They consist of a rubber tube covered by an inextensible nylon braid.



Figure 5. Schematic view of the air muscle

These muscles are characterized by a high force to weight ratio, which equals 400:1. For comparison, this ratio for a commonly used electric motor equals 16:1. Pneumatic muscles usually work under pressure between 0 and 5 bars. They can be directly attached to the construction or transfer the force by a system of tendons. Driving a lever is a basic application for artificial muscles. This situation is presented in picture Fig.6.

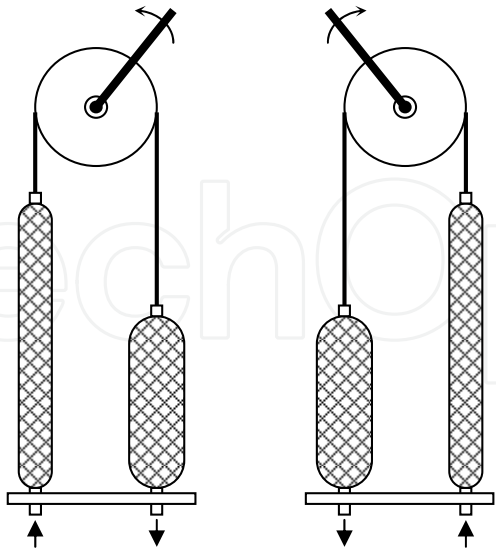


Figure 6. Lever movement driven by a pair of McKibben muscles

Since the artificial muscle can generate only a contracting force similar to real ones, a pair of such actuators is needed. One works as the agonist while the second one as the antagonist force generator

In order to generate movement of the lever to the left, the muscle on the left must be filled with compressed air. The right muscle must be empty during that same time. In order to generate the backward movement, an opposite situation must occur. The right muscle has to be filled while the left one releases air.

7. Considerations on the static parameters of artificial muscles. (Chou C.P., Hannaford B., 1996)

An artificial muscle is an element in which pneumatic or hydraulic energy is transformed into mechanical energy.

In order to solve the relation between pressure and generating force, the rule of transformation of energy is taken into consideration.

When compressed air presses on the internal walls of the rubber tube, the gas performs work.

$$dW_{in} = \int_{S_i} (P - P_0) dl_i ds_i = (P - P_0) \int_{S_i} dl_i ds_i = P' dV \quad (1)$$

Where

P- inner pressure

P0- atmosphere pressure

P' - absolute pressure

dli - increment of length

Si - total internal surface

dV - increment in volume

External work produces a force combined with the shortening of the muscle length

$$dW_{out} = -FdL \quad (2)$$

Where:

F - tension

dL - displacement in length.

The principle of conservation of energy shows that the delivered work in the compressed air equals the exterior work.

$$dW_{out} = dW_{in} \quad (3)$$

Transforming equation (3), receive:

$$F = -P' \frac{dV}{dL} \quad (4)$$

In order to calculate the dV/dL some assumptions have to be made. The first is that when expanding the braid of fibers the Volume of tube depends only on its length. The second is that the active part of the muscle is modeled as a perfect cylinder. This situation is shown on the picture Fig.7.

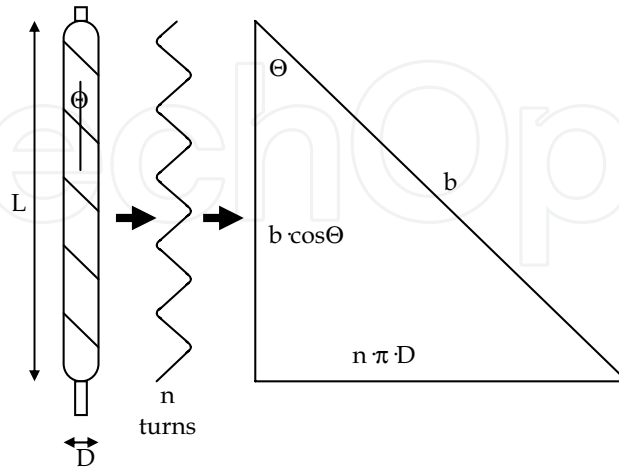


Figure 7. Schematic of the muscle's braid analysis

L - represents the length of the cylinder, D its diameter and the θ represents the angle between the longitudinal axis of the muscle and braid fibers. The character b is the length of the fiber and n is a number of rotations around the rubber tube. The parameters l and D may be calculated by equations

$$l = b \cos \theta \quad (5)$$

$$D = \frac{b \sin \theta}{n \pi} \quad (6)$$

On this basis the volume of the cylinder is represented by the equation (7)

$$V = \frac{1}{4} \pi D^2 L = \frac{b^3}{4 \pi n^2} \sin^2 \theta \cdot \cos \theta \quad (7)$$

Taking in to consideration the formula (4) and replacing there variable V , the equation described by (8) results in:

$$F = -P \frac{dV}{dL} = -P \frac{dV/d\theta}{dL/d\theta} = \frac{P b^2 (2 \cos^2 \theta - \sin^2 \theta)}{4 \pi n^2} = \frac{P b^2 (3 \cos^2 \theta - 1)}{4 \pi n^2} \quad (8)$$

With some simplifications the formula of the force may be represented as (9)

$$F = \frac{\pi D_0^2 P'}{4} (3 \cos^2 \theta - 1) \quad (9)$$

Where $d_0 = b/n\pi$ is the diameter, while the angle of the net is 90 degrees.

Taking into analysis equation (9), the maximum shortening occurs when the force F reaches the value 0. This takes place while the θ equals 54,7 degrees.

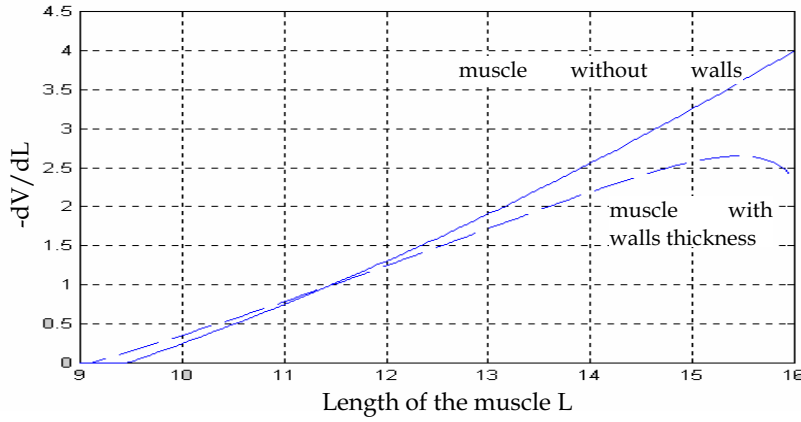


Figure 8. Theoretical characteristic of muscle force with/without walls taken into considerations

Considering the wall thickness as a parameter in all formulas, the final rule describing Force dependant of the pressure, may be represent by the equation (11)

$$V = \frac{1}{4} \pi (D - 2t_k)^2 L \quad (10)$$

Sample characteristics calculated with a $b=16.4\text{cm}$ and $n=3.15$ are presented in Figure 8.

$$F = -P' \frac{dV}{dL} = \frac{\pi D_0^2 P'}{4} (3 \cos^2 \theta - 1) + \pi P' \left[D_0 t_k \left(2 \sin \theta - \frac{1}{\sin \theta} \right) - t_k^2 \right] \quad (11)$$

Analysis of equations (9)(11) shows that a force generated during statical expansion is proportional to the muscle shortening. This function descends with the shortening in length. It requires the initial condition of full extension of the muscle increasing the range of linear work. Application of artificial muscles in construction of the hand is a reflection of natural method of finger movement generation. Similar to Imitating the nature the presented hand has all muscles placed in a forearm part connected to fingers with tendons. All applying muscles have their standard length of 150mm in a full extension. They shorten by about 30mm when they are fully filled up with compressed air. Nominal supplying pressure for them is 4 bars producing a force of about 30N. In this work they were supplied with 6 bars. This condition obviously increases the maximum force, but reduce the lifetime of the muscle.

8. Kinematics model of the artificial hand.

Creating the vision system in a control feedback loop is based on the knowledge of fingertip trajectories referred to as the base markers. All curved lines representing the paths of the makers can be calculated with a Denavit-Hartenberg notation (Jezierski E., 2002). This rule allows solving a forward kinematic task. A position of any point of a mechanical structure

can be found only with the knowledge of the angle of rotation joints and the linear translations between them.

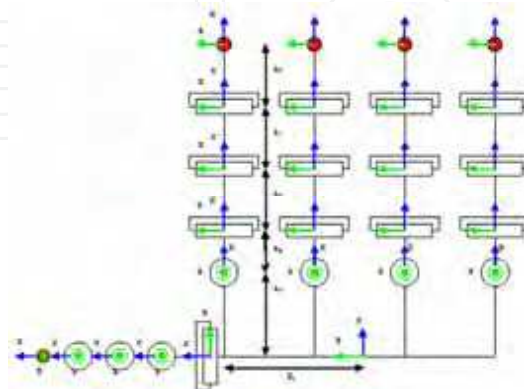


Figure 9. Kinematic model of the hand

The mathematical model presented on Fig.9 reflects the kinematic structure of the constructed hand. The joints of the wrist are ignored because they are not considered in calculations. The created hand has some simplifications in comparison to the presented model because some of the joints are blocked to reduce the number of Degrees Of Freedom. In order to calculate the 3-D position of every joint, the transition matrix A has to be solved. Transition between two points in 3-D space described by translation and rotation can be calculated by the equation:

$${}^{i-1}\hat{r} = A_i {}^i\hat{r} \quad (12)$$

Matrix A represents four mathematical operations:

1. Rotation around Z axis
2. Translation along Z axis
3. Translation along X axis
4. Rotation around X axis

These operations may be represented by equation (13)

$$A_i = \text{Rot}(Z, \theta_i) \text{Trans}(0, 0, d_i) \text{Trans}(a_i, 0, 0) \text{Rot}(X, \alpha_i) =$$

$$= \begin{bmatrix} \cos \theta_i & -\sin \theta_i & 0 & 0 \\ \sin \theta_i & \cos \theta_i & 0 & 0 \\ 0 & 0 & 1 & 0 \\ 0 & 0 & 0 & 1 \end{bmatrix} \begin{bmatrix} 1 & 0 & 0 & 0 \\ 0 & 1 & 0 & 0 \\ 0 & 0 & 1 & d_i \\ 0 & 0 & 0 & 1 \end{bmatrix} \begin{bmatrix} 1 & 0 & 0 & a_i \\ 0 & 1 & 0 & 0 \\ 0 & 0 & 1 & 0 \\ 0 & 0 & 0 & 1 \end{bmatrix} \begin{bmatrix} 1 & 0 & 0 & 0 \\ 0 & \cos \alpha_i & -\sin \alpha_i & 0 \\ 0 & \sin \alpha_i & \cos \alpha_i & 0 \\ 0 & 0 & 0 & 1 \end{bmatrix} \quad (13)$$

The final equation for the A matrix is as follows:

$$A_i = \begin{bmatrix} \cos \theta_i & -\sin \theta_i \cos \alpha_i & \sin \theta_i \sin \alpha_i & a_i \cos \theta_i \\ \sin \theta_i & \cos \theta_i \cos \alpha_i & -\cos \theta_i \sin \alpha_i & a_i \sin \theta_i \\ 0 & \sin \alpha_i & \cos \alpha_i & d_i \\ 0 & 0 & 0 & 1 \end{bmatrix}$$

(14)

Transformation from the 3-D reference position to an effector coordinates may be solved using (15):

$${}^0\hat{r} = A_1(q_1)A_2(q_2)...A_n(q_n)^n\hat{r}$$

(15)

All dimensions and relations required to determine the finger tip position are presented in Table 1. All translations are given in millimeters and rotations are in radians.

Finger 1				Finger 2			
a _i	α _i	d _i	θ _i	a _i	α _i	d _i	θ _i
85	π/2	42	0	85	π/2	17	0
0	-π/2	0	0	0	-π/2	0	0
45	0	0	0	45	0	0	0
40	0	0	0	40	0	0	0
40	0	0	0	40	0	0	0
Finger 3				Finger 4			
a _i	α _i	d _i	θ _i	a _i	α _i	d _i	θ _i
85	π/2	-17	0	85	π/2	-42	0
0	-π/2	0	0	0	-π/2	0	0
45	0	0	0	45	0	0	0
40	0	0	0	40	0	0	0
40	0	0	0	40	0	0	0

Thumb			
a _i	α _i	d _i	θ _i
1	π/2	45	0
30	-π/2	0	0
45	0	0	0
40	0	0	0
30	0	0	0

Table 2. Kinematic parameters of the finger joints in Denavit-Hartenberg notation

The kinematic model is used to determine the points of finger tip trajectories. These points are calculated in two situations. First one shown in Fig.10.a) represents the side view of the

hand, while the second in Fig.10.b) represents the front view. Those curved lines are useful in vision analysis, because the whole operation of locating fingertip markers can be reduced to searching only along selected lines (Jezierski E. Zarychta D. 1995). The real curves are only slightly different from the theoretical ones, which are obtained by assuming equal revolutions in all the joints. This difference however cannot be entirely neglected so appropriate corrections have to be made.

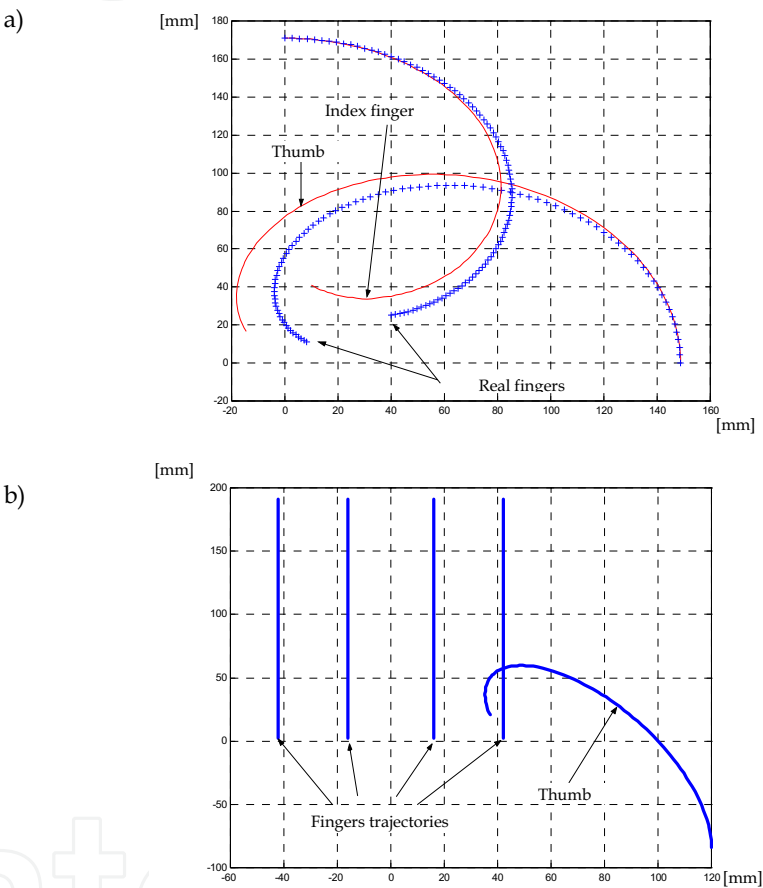


Figure 10. Model characteristics of fingers trajectories in side (a) and front (b) view

Trajectories of the fingertips are presented in Fig. 10. The main disadvantage of the frontal camera view is the lack of possibility to predict perspective distortions. Without these corrections modeling of the fingertips is a simplification and results in obtaining a very inaccurate approximation of the position of the finger tip markers.

Determining the trajectory of the thumb in a general case is complicated because its end traces a curved plane in 3-D space. This is the result of an additional joint, which allows rotation in the plane perpendicular to the palm surface. The shape of the curved plane marked by the thumb tip is presented on Fig.11.

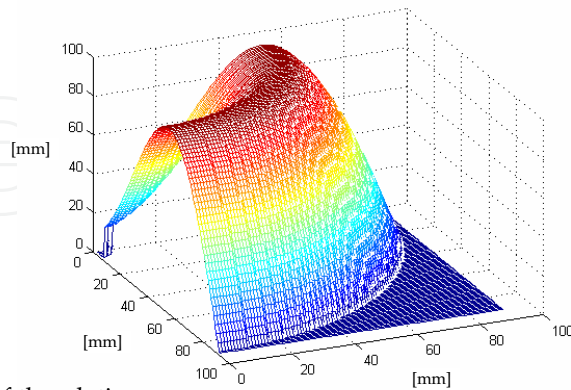


Figure 11. 3-D range of thumb tip

Vision control used for recognition of finger positions scans along specified trajectories instead of analyzing the whole image. This method speeds up the analysis process, allowing it to be implemented on slower computers. The trajectories calculated from the kinematical model are placed on the captured view. They are scaled to the hand size on the picture by two base markers.

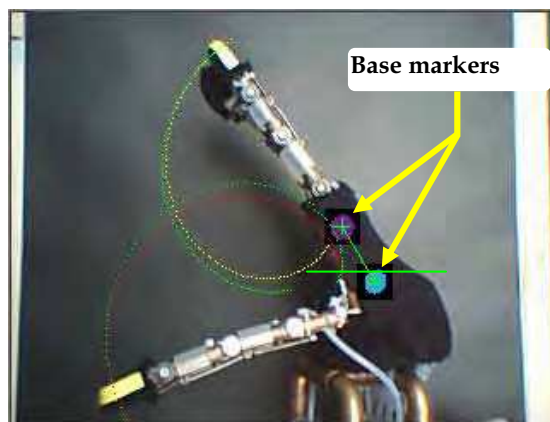


Figure 12. Artificial hand side view with base markers

The distance between these markers on the picture and in reality allows to determine the scaling coefficient (16)

$$k = \frac{\sqrt{(x_{b2} - x_{b1})(x_{b2} - x_{b1}) + (y_{b2} - y_{b1})(y_{b2} - y_{b1})}}{d} \quad (16)$$

$$x' = x \cdot \cos \theta + y \cdot \sin \theta \quad (17)$$

$$y' = -x \cdot \sin \theta + y \cdot \cos \theta \quad (18)$$

$$x'' = x_b + k \cdot x' \quad (19)$$

$$y'' = y_b + k \cdot y' \quad (20)$$

Where :

θ - angle between the line connecting the base markers and the horizontal line passing through the bottom marker

$x_{b1}, x_{b2}, y_{b1}, y_{b2}$ pixel coordinates of base markers on the screen.

Scanning lines are fit to the markers and scaled by the k ratio. Moreover, the base points are useful in calculations of hand orientation. The wrist of the hand can also be moved, so the tilt of the palm may change. Identification of the position of these markers is performed by scanning the area around them. If the cursor changes its position significantly inside the scanning range, a new position of the searching area is determined for next scan. Center of the region overlaps with the center of the base marker. This approach also reduces the number of operations required for vision analysis.

Increasing contrast in the captured view and placing bright markers on a dark background allows quick identification of their position. All trajectories are determined with a 1 degree resolution. Every marker commonly covers more than 2 points of these curves. Calculating the center of the cursor along the scanning line permits identification of every joint's angle.

9. Methods of grasp recognition

Two methods of grasp recognition were utilized (Kaczmarek M., Zarychta D., 2005). The first one focuses on precision and a soft touch. At each image refresh the distance between the edge of a marker and the nearest object point is measured. In the case when the angular distance is less than 4 degrees the signal for the confirmation of the grasp is sent. Such situation however is definitive only in a limited number of cases i.e. in the case of cylinders or cubes. The grasp of e.g. a cone or a pyramid when the base is directed towards the camera can cause a misinterpretation. In a side view only the two-point grasp can be applied. The main cause of this situation is the occluding of the fingers by the nearest one.

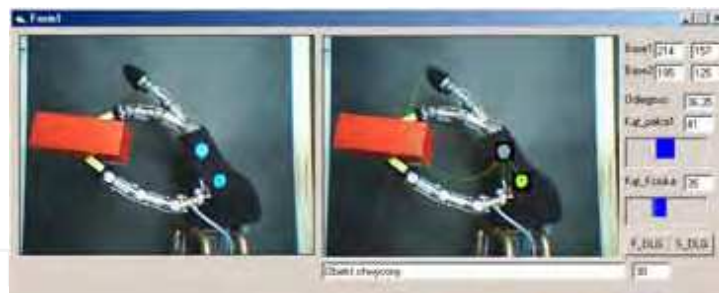


Figure 13. Control program interface

Another approach providing a strong and steady grasp is a time-position analysis. With every refresh of a captured view the positions of all fingers tip markers are calculated. If their position differs from the previous view, the compressed air is pumped to the muscle. If the finger stays in the same position despite the activation for further movement it means that an obstacle is located in its way. After a few ineffective attempts to continue the movement the situation is interpreted as a firm contact. The muscle stops filling up with compressed air. Time analysis allows a correct grasp in the case when the object is not placed directly on the scanning line. Blocking one of the finger sections by the object can

prevent observation of the changing of position of the finger tip, which the control algorithm will interpret as the grasping of the obstacle. This also causes the electro-valves to close. This kind of approach is perfectly suitable for situations where the application of a larger force is needed. It can be used to move small obstacles or to push buttons.

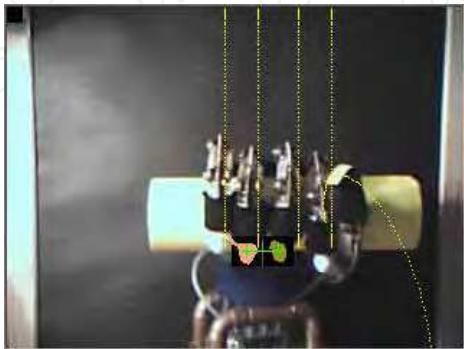


Figure 14. Grasping of a cylinder

Regarding the particular character of the created construction, only the type of grasp with distal segments can be used (Kang S.B., Ikeuchi K., 1992). Presenting considerations referring to the front view, when the camera is placing towards to the hand. This situation allows for shape analysis of the manipulated object, and adapting the finger position to the gripped body. Foundation of this task was that the object can not rotate during catching, and the object is homogenous. These assumption causes that the grasp must be applied precisely.

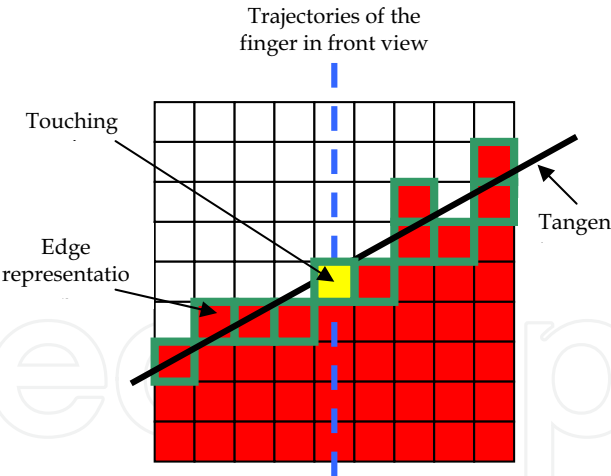


Figure 15. Edge analysis

Perfect for this task is the algorithm that measures the distance between the finger and the object. Applying it causes the fingers to gently touch the edge of the object, without having any influence on its position. Considering the small differences in the muscles and electro-valves constructions and shape of the object, the time of touching the object depends of the

finger construction and the distance between the object and fingertip. Other type of grasp, such as a time-position analysis, could cause a rotation of the grasped body, resulting in a different time of touching and an unbalanced distribution of force. When all fingers gently reach their position the force can be increased, because the distribution of force produces zero momentum of rotation. Only now the grasped object can be lifted.

In calculations of the touching points to the object the distribution of the moments of rotation is considered. The only information obtained from the captured view is the shape of the object and the position of the fingertip markers.

The center of mass of an object view can be calculated under the condition that the grasping body is homogenous. Only this assumption allowed for calculating the 2 dimensional representation of the position of an object's center of mass (Tadeusiewicz R., 1992). Assuming that all the fingers act with the same pressure the counter position of the thumb can be calculated.

Around the contact point, the tangent to the shape edge is calculated (Figure 15). The size of the area where the tangent is calculated is determined by a square with 9x9 pixels. Analysis of the pixels belonging to the object and in the contact point allows for calculating the tangent and the distribution of force. This force produces the torque. In all the calculations the method of the sum of least squares is used. This is represented by equations (21)(22)(23)(24)

$$y = a_0 + a_1 \cdot x \quad (21)$$

Coefficients a_0 and a_1 are determined by (21)(22)

$$a_0 = \frac{1}{D} \begin{vmatrix} \sum y_i & \sum x_i \\ \sum x_i y_i & \sum x_i^2 \end{vmatrix} \quad (22)$$

$$a_1 = \frac{1}{D} \begin{vmatrix} n & \sum y_i \\ \sum x_i & \sum x_i y_i \end{vmatrix} \quad (23)$$

$$D = \begin{vmatrix} n & \sum x_i \\ \sum x_i & \sum x_i^2 \end{vmatrix} \quad (24)$$

Where :

y_i, x_i are the pixel coordinates

n - number of pixels taken to calculations

Those calculations determined for every finger helps to predict the position of the thumb. Distribution of the force during grasping with a position of the thumb for various objects is shown on Fig.16.

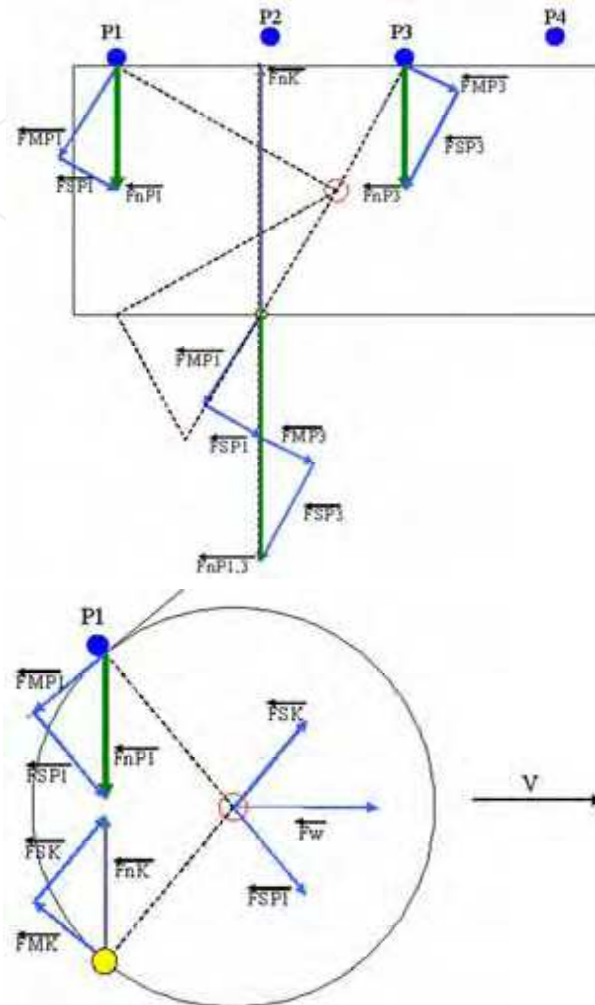


Figure 16. Distribution of forces acting on an object

Analysis of a rounded object with a two finger grasp shows that even if the torque equals zero, there is an unbalanced horizontal force which makes an object slip out from the grasp. To perform correct hold at least three fingers must stay in contact with the object. Moreover, they should be placed symmetrically to the center of mass. Only this kind of arrangement of finger positions allows the object to stay motionless during grasping.

10. Results of experiments

All situations presented on the figures 17-21 show the control program during grasp analysis for objects of different shapes. During this, two, three, or four fingers can participate. Screens show how the shape of the objects influences the fingertip positions. For a single shape only the final stage of grasping is presented.

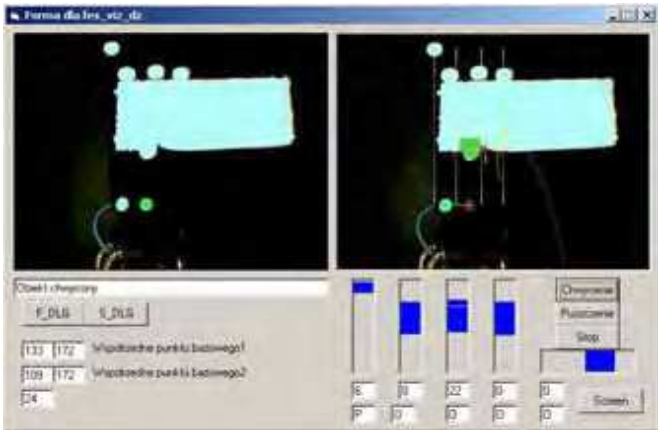


Figure 17. Grasping a cuboid

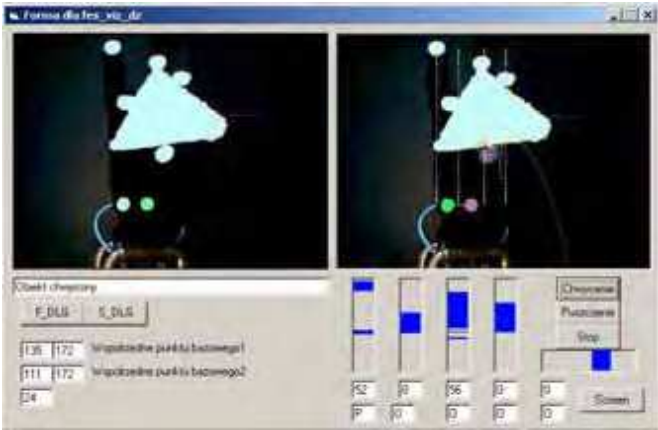


Figure 18. Grasping a cone

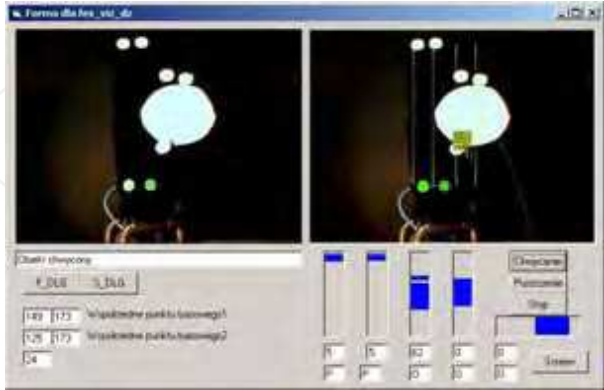


Figure 19. Grasping a sphere

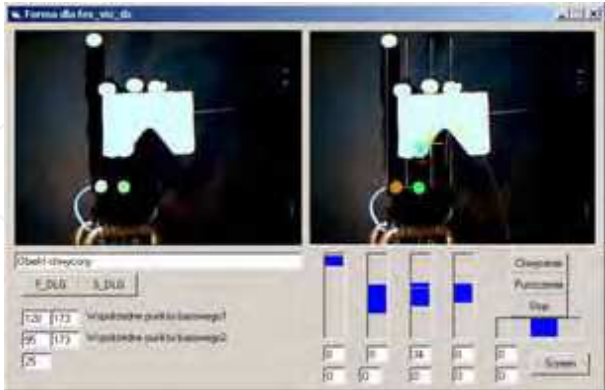


Figure 20. Adaptive grasp

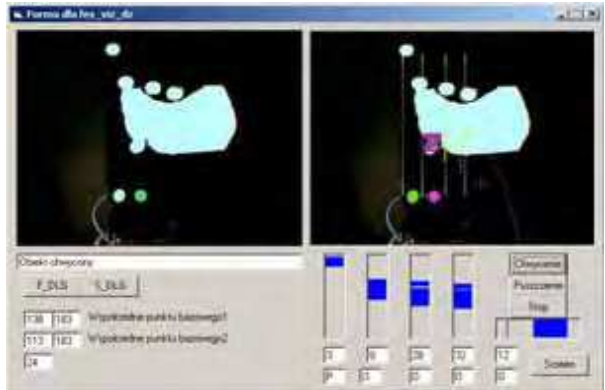


Figure 21. Adaptive grasp

Presented results show that the applied algorithm is well suitable for grasping of objects of unknown shape. It can be used with more than just the typical bodies such as a cuboid, cone, pyramid or a sphere. The presented pictures show that the fingers are able to adapt to the body in the way which doesn't produce a rotation during holding. Vision control which is put into practice has some disadvantages. In this work there was no correction for the perspective distortion of the camera. The deviation produced by the camera didn't significantly affect the control of the artificial hand's fingers' positions, so the distortion could be neglected.

11. Myopotential control for an artificial hand

Human hand including the wrist contains 22 Degrees Of Freedom. This number shows how complex are its manipulation capabilities. Research works are not only aimed at adapting artificial grippers into mobile platforms or humanoid robots, but they are also focused on prosthetic products for amputees of fragments of the upper limb. The mechanical construction of such prosthesis does not cause great problems, however the increasing of the number of degrees of the freedom complicates the control system. The prosthesis of the hand should be characterized by a number of degrees of the freedom being enough for the

realization of basic motor functions of hand, as well as it should be close with the shape and the weight to the lost fragment of the upper limb.

For persons after amputations, electromyographic signals of human muscles are using for steering the bioprosthesis. In most cases 4 classes of states of the hand are determined, but research works at the Technical University of Wroclaw allow for isolation of even 9 classes. Analysis of potential movement possibilities of artificial hand, shows that the construction of a hand containing a number of DOF similar to a real hand is impractical, because using only 9 states classes for the palm some of the joints would be useless. That's why most of the bioprosthesis contains only three movable fingers or thumb with a pair containing two fingers in each group. This kind of widely applied three finger bioprosthesis has been made in the Oxford Orthopedic Engineering Center.

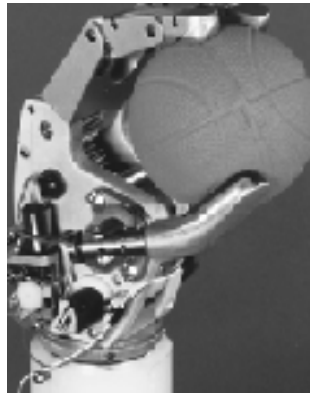


Figure 22. Bioprosthesis from the Oxford Orthopedic Engineering Center

(Oxford University Gazette, 1997) *“Designed to function as a prosthesis for people who do not have a hand, it is controlled by a small computer contained within it. The hand uses low-level signals generated by the user flexing muscles in the forearm, and translates them into action.*

Dr Peter Kyberd, a researcher at the Department of Engineering Science, who led the team which developed the hand, said: ‘The most important thing about a hand prosthesis is that it should be as easy to wear as a pair of glasses. You just put it on in the morning and use it without thinking about it.’

The user of the hand can give three basic instructions: open, close, and grip. What makes the device unique is that sensors inside it allow it to decide what grip shape to adapt and how hard to squeeze. If it feels an object slipping, it will automatically grip harder without the user's intervention.”

The inspection of similar structures includes „Sensor Hand TM” of the company Otto Bock, the artificial DLR hand from Germany, Japanese structure from Complex Systems Engineering from the Hokaido University, and the Mitech Lab bioprosthesis from Italy.

Despite of anthropomorphic construction used for bioprosthesis (Wołczowski A., Kowalewski P., 2005) five fingers hands for special tasks are also designed. Future robots will work together with humans, so their grippers must be adapted to operating human tools. Therefore their effectors must be similar to and as dexterous as a human hand. An example of such project is the NASA “Robonaut” robot (NASA RoboNaut Project), which is supposed to perform maintenance tasks outside the space station. His artificial hands are similar to human ones, and an advanced control algorithm permits for complex movements such as screwing on nuts.



Figure 23. “RoboNaut” hands – Nasa project

On account of the noninvasive character of muscle mipo-potential measurement, an active electrode for biosignals recording has been designed (Clark J.W. 1978). Imperfection of this kind of recordings results from the activation of a wide group of muscles. An invasive method would be able to measure the activation of a single motor unit. Reduction of artifacts in the bioelectric signal is performed by placing contact electrodes close together (10mm), parallel to muscle fibers, that the interferences of other muscles don’t significantly affect the measured signal. Additionally, an active electrode is supplied in a third contact point, which reduces the influence of external power line interferences.

12. Interference reduction by Right Leg Drive system.

Common mode voltage in measurement by a two contact electrode can be performed in several ways.

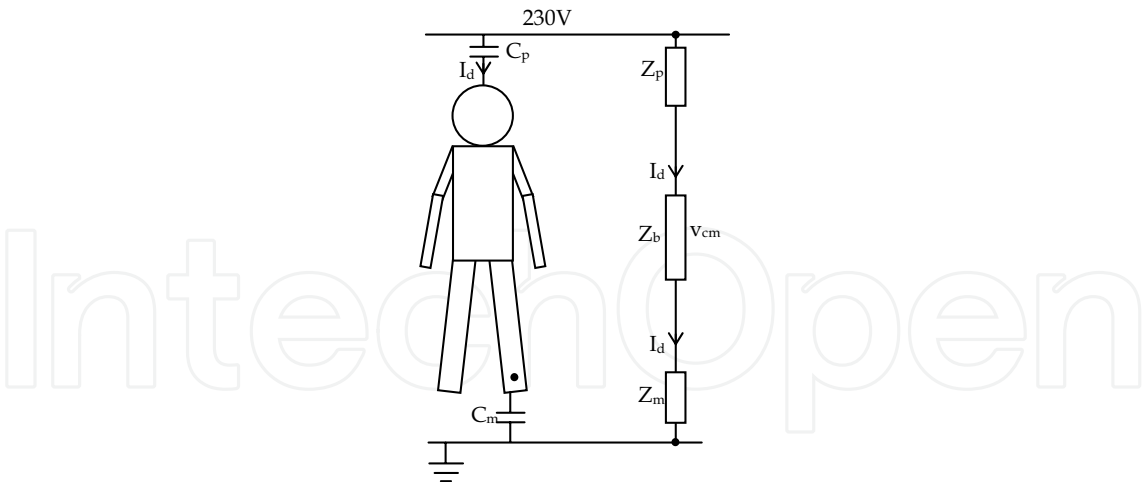


Figure 24. Simple electronic equivalent circuit of human body in electromagnetic field

Electric equivalent circuit of the human body surrounded by an electric field from power lines, shows that a leakage current flowing from the power line to the ground. This current is the consequence of a finite impedance Z_p , which can be considered as a capacitance

between a power line and a human body. It flows through impedance of the body Z_b and impedance between the body and the ground Z_m , causing appearance of a common mode voltage on both surface electrodes. Both impedances Z_m and Z_p are larger compared to the value of Z_b . The amount of the common mode voltage depends on the proportion between Z_p and Z_m . In the worst case condition, when breakdown voltage of the power line occurs on the human body the reduction of the shocking impulse current depends only on the isolation Z_m between the body and the ground. Unfortunately, to reduce the common mode voltage, this impedance should stay low in order for the potential of the ground of the electric circuit to be comparable to the ground potential of the examined patient. The best solution would be connecting the patient to the potential of the ground. However this situation requires special conditions preventing electrical shocking. Moreover in this situation, the instrumentation amplifier's CMRR parameter (Common Mode Reduction Ratio), which should be very high between 100dB-120dB, can only reduce the value of the common mode voltage.

Today the common application for reducing the common mode voltage is the application of a negative feed-back loop (Metting van Rijn A.C., Peper A., Grimbergen C.A., 1990). The patient is connected by a third electrode where a negative and amplified V_{cm} voltage is presented. This solution allows for reduction of the common mode voltage without decreasing the value of the ground isolation Z_m . The negative feed-back loop produces a reference point for biopotential measuring, the level of which is comparable to the ground level of the electric circuit. The electric equivalent circuit is presented on Fig.25.

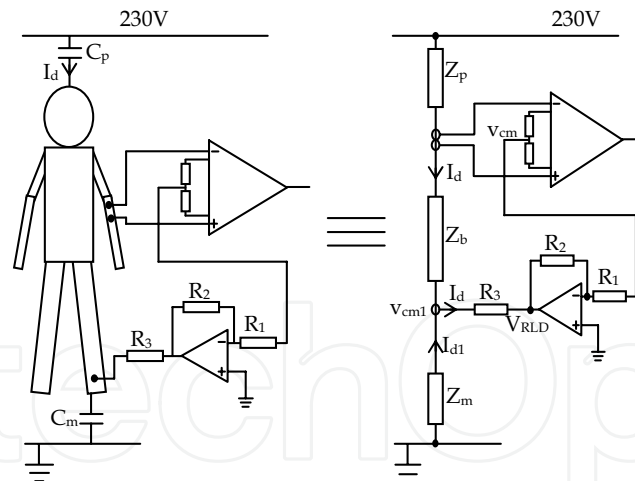


Figure 25. Electronic circuit for interference reduction

Considering relations (25)(26) in this circuit, a rule for reducing a common mode voltage occurs (31). It decreases as much as the gain value of feed back loop increases.

$$V_{cm} = I_d \cdot R_b + V_{cm1} \quad (25)$$

$$V_{cm1} = V_{RLD} + I_d \cdot R_3 \quad (26)$$

$$V_{RLD} = -V_{cm} \frac{R_2}{R_1} \quad (27)$$

$$V_{cm} = I_d \cdot R_b + V_{RLD} + I_d \cdot R_3 \quad (29)$$

$$V_{cm} - V_{RLD} = I_d \cdot (R_b + R_3) \quad (28)$$

$$V_{cm} \left(1 + \frac{R_2}{R_1} \right) = I_d \cdot (R_b + R_3) \quad (30)$$

$$V_{cm} = I_d \cdot (R_b + R_3) \left(\frac{R_1}{R_1 + R_2} \right) \quad (31)$$

Moreover this solution has also a safety advantage. When an electric shock occurs and the patient is isolated from the ground, the feedback amplifier saturates. On its output a negative potential occurs. The shocking current I_d flows through a resistance R_3 to the ground. Typically the value of R_3 is 390k Ω , which reduce this current to a safe value.

13. Description of an active electrode

In order of perform the best collection of the EMG signals, the conditional circuit should be placed as close as possible to the measuring pads. This circuit consist of an instrumentation amplifier and a second order band-pass filter. The high input impedance and a high value of CMRR 110-120dB characterize the used amplifier INA128. These two parameters are the key for a common mode voltage reduction. The band pass filter has a low cut-off frequency set to 10Hz and a high cut-off frequency of 450Hz. This range provides correct measurement in a full bracket. Cutting the low frequencies removes all artifacts which may appear as a consequence of small movements of the electrode pads on the skin. Moreover a high pass filter rejects the offset voltage and provides transformation to a fully bipolar type of the signal. The low-pass filter removes the high frequency signals which are produced by most electronic devices such as D.C. converters. These useless frequencies could be measured by an analog to digital converter and they may affect the frequency spectrum of the biopotentials.

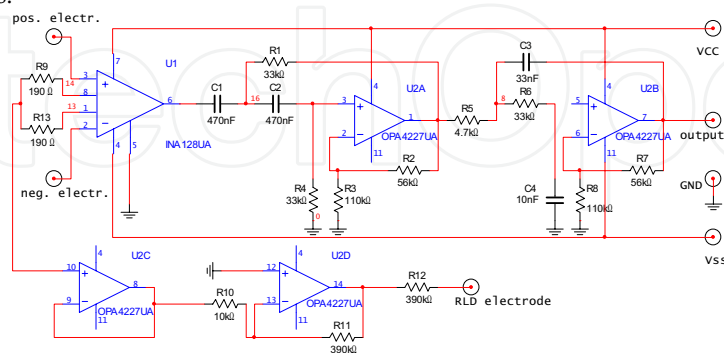


Figure 26. Electronic circuit of surface active electrode for biopotential recordings

Moreover a presented active electrode also contains an RLD circuit which is used for decreasing of the common mode voltage and which is connected to a third pad of the measuring unit. Picture 27 presents real view of the electrode and it's electrical circuit is shown on the figure 26. The size of the electrode is 20mm x 30mm. All 3 silver contact pads are 10mm long and 1mm wide. They are also separated by a distance of 10mm.

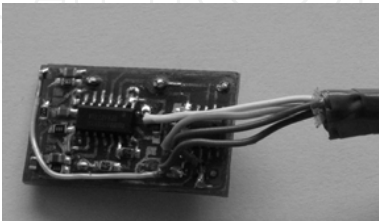


Figure 27. Real view of the active electrode

14. Description of the measuring path.

The active electrode is connected to a measuring path where the biopotential signal is further transformed and relayed to the computer. The most important part of this conditioner is the isolation unit. This device provides a safe level of voltage on the patient side. Its task is to isolate the electrode and the examined patient from potential electrical shocking. Additionally, this measuring path contains another low pass filter to increase the dumping value and a voltage level shifter on the input of the analog to digital converter. Since the amplitude of electromyographic signal is at a level of 500-1000 μ V , the conditioning path provides an amplification to raise the amplitude to the range of 500-1000mV. The Amplitude-Frequency characteristic of an EMG measuring path is presented on the picture below.

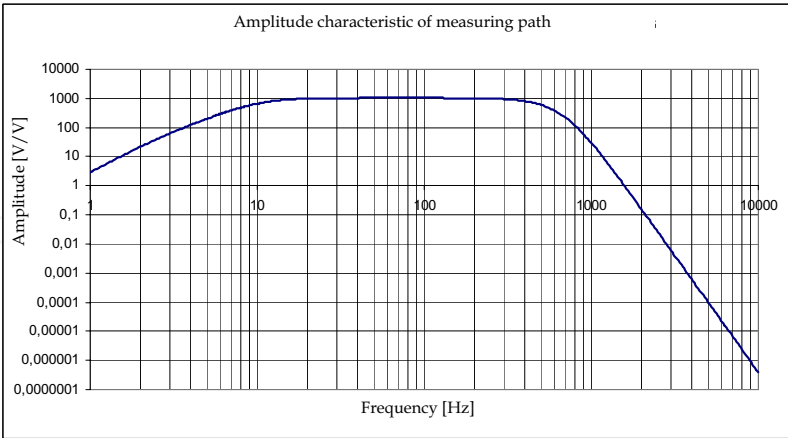


Figure 28. Filter frequency characteristic

Measuring of the biopotential signal with an active electrode put above the flexor digitorum superficialis muscle is presenting on the image Fig.29.

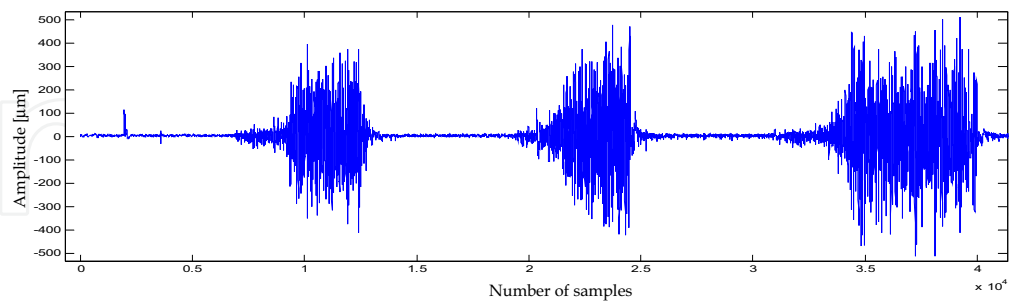


Figure 29. Electromyogram of examined muscle

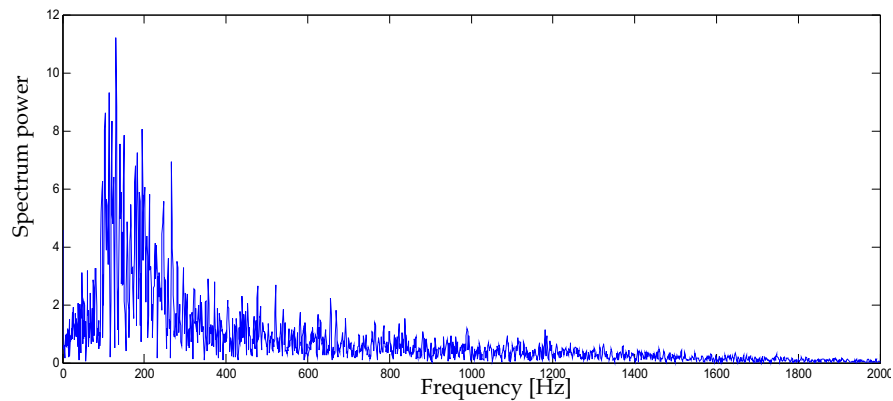


Figure 30. Fourier transformation of the muscle's response to stimulation

The control of the artificial hand by a biopotential signals is performed on the laboratory stand which diagram is presented on Fig.31.

An active electrode placed over the group of examined muscles measures the electric potential. Then the signal is amplified and filtered to the useful range of frequencies 10-450Hz. In the next step, the signal is acquiring by an A/D converter and filtered in order to remove the 50Hz power line frequency. This filtration is performed by a digital algorithm. After these operations, the control program calculates the root mean square value of the received waveform. This calculation is performed after every 10ms of received data. However, a spectrum analysis is performing with a 1s refresh. The RMS value is a basic information showing the level of muscle tension. This information is applied to the function, which converts the level of muscle activation into the air pressure level. Another control algorithm, which uses a two-step regulator with a dead zone, provides stabilization of the air pressure in the McKibben muscles. If the pressure is lower than a minimum threshold, the electrovalves pump air into the muscle. When the pressure exceeds the specified limits another electro-valve releases the air from the muscle. Experiments performed with this control method show that using only one electrode it is possible to obtain a simple close-open movement with a few different bending states.

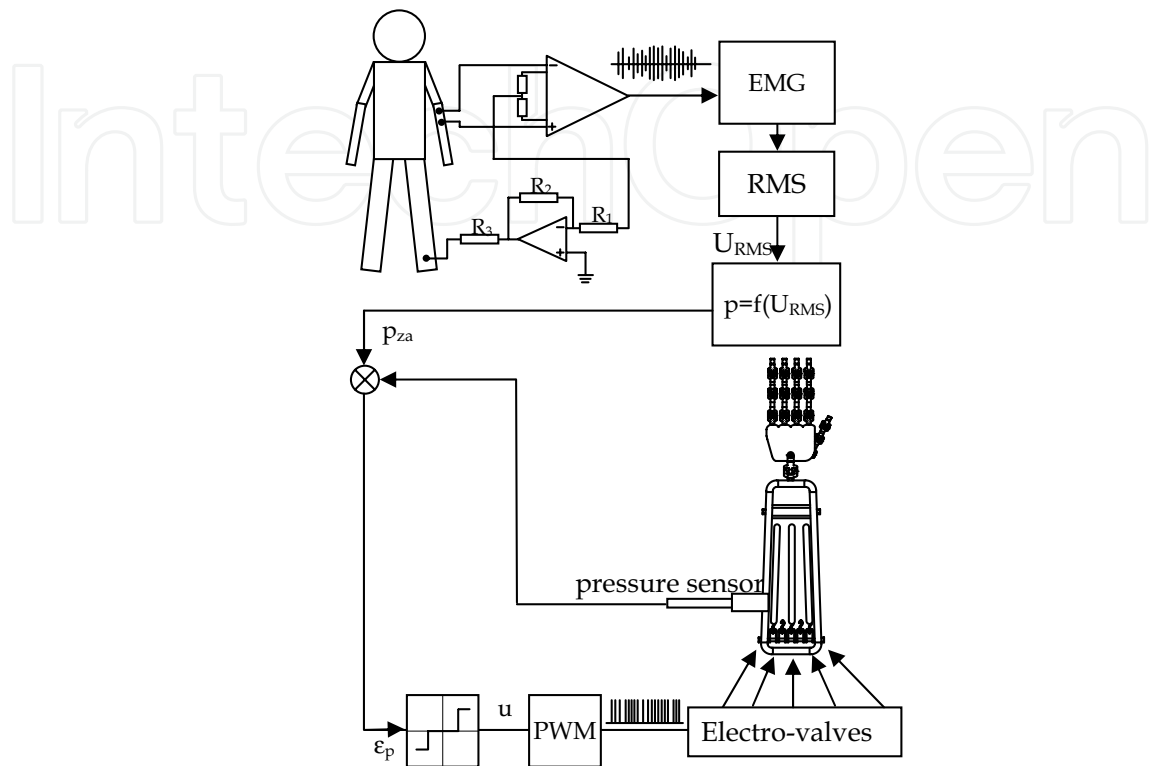


Figure 31. Laboratory stand schematic

15. Conclusions

This work presented aspects connected with the structure and control of a five finger, anthropomorphic gripper, working under the supervision of a vision system. The presented construction is characterized by some simplifications in comparison to the real human hand, as it has only 9 Degrees Of Freedom. However, those limitations do not reduce its grasping possibilities, which was shown in the paper. This hand had no problem with grasping objects of different shapes by adapting the position of fingertips to the shape of body edge. The mechanical construction has an additional DOFs which could make its manipulating possibilities closer to the human hand; however, they are blocked to simplify the algorithms of the vision control feedback loop. Examples presented in the paper based on some simplifications in the vision control algorithm. Perspective distortions were not addressed, because in the scanning line method where the curve trajectories are fitted to the hand view, the deviation value was negligible. The presented observation of the artificial hand for two locations of the camera cause big limitations of control. There is a possibility of the ambiguity of solutions in the thumb position analysis.

The designed and presented research position has essential teaching advantages, which allow for testing algorithms with vision control in the feedback loop in a wide range. Moreover, the artificial hand can be installed on a robotic arm, which increases its

manipulating possibilities. Another expansion of the artificial hand construction may be installation of additional sensors of force and temperature, which would make this hand more similar to a human limb.

The presented control method uses basic electromyographic signal analysis. Although it determines the tension of the examined muscle group it is not sufficient for full analysis of the examined patient's intentions. In the future works an attempt of computerized identification of strength of muscles will be taken. This identification will base on the multipoint EMG measuring system, which allows to determine correlation between the muscle groups in the different finger postures (Krysztoforski K., Wołczowski A., Busz S., 2005). The mathematical model created on this base permits much more precise steering and identifies the patient's intentions.



Figure 32. Real view of hopping robot leg

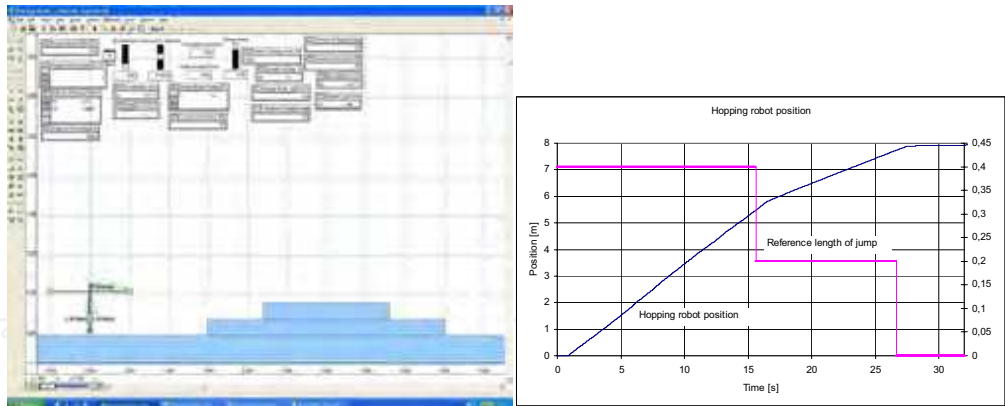


Figure 33. Simulations of jumps in uneven terrain and plot of Hopping robot position

Additionally, an attempt of leg muscle identification during a vertical jump will take place. This information will be used for a jumping robot (Fig.32)(Fig.33), which task is freely jumping on uneven terrain performing human-like leaps. Tentative simulations show that a mathematical description of the hopping robot permits for balancing jump control of the mechanical equivalent of a human leg (Raibert M.H., 1986). This research was partially financed by Ministry of Science and Higher Education under grant No 3 T11A 023 30 and 3

T11A 024 30. Moreover, the created leg may also be adapted as an exoskeleton, which would support the walking process. For this task myopotential signals are used for identification of walking intensions of an examined patient.

16. References

- Clark J.W. (1978), *Medical instrumentation, application and design*, Houghton Mifflin, Boston.
- Jezierski E. (2002), *Robotyka kurs podstawowy*. Wydawnictwo PŁ, Łódź.
- Raibert M.H. (1986), *Legged robots that balance*, The MIT Press.
- Tadeusiewicz R. (1992), *Systemy wizyjne robotów przemysłowych*. WNT Warszawa.
- Chou C.P., Hannaford B. (1996), Measurement and Modeling of McKibben Pneumatic Artificial Muscles. *IEEE Transactions on Robotics and Automation*, Vol. 12, No. 1, pp. 90-102.
- Feja K., Kaczmarowski M., Riabcew P. (2005), Manipulators driven by pneumatic muscles, *CLAWAR 8th International Conference on Climbing and Walking Robots*, pp. 775-782, London UK.
- Jezierski E. Zarychta D. (1995), Tracking of moving robot arm using vision system. *SAMS*, Vol. 18-19, pp. 534-546.
- Kaczmarowski M., Zarychta D. (2005), Vision control for an artificial hand, *CLAWAR 8th International Conference on Climbing and Walking Robots*, pp. 623-630, London UK.
- Kang S.B., Ikeuchi K. (1992), Grasp recognition using the contact web. *Proc. IEEE/RSJ Int'l Conf. on Intelligent Robots and Systems*, Raleigh, NC.
- Krysztowski K., Wołczowski A., Busz S. (2005), Rozpoznawanie postury palców dłoni na podstawie sygnałów EMG, *Proceedings of VIII-th National Conference of Robotics*, T2 pp. 213-220, Wrocław.
- Metting van Rijn A.C., Peper A., Grimbergen C.A. (1990), High-quality recording of bioelectric events, *Med. & Biol. Eng. & Comput*, 28, 389-397.
- Wołczowski A., Kowalewski P. (2005), Konstrukcja antropomorficznego chwytaka dla zręcznej bioprotezy dłoni. *Proceedings of VIII-th National Conference of Robotics*, T2 pp. 193-202, Wrocław.
- NASA RoboNaut Project. Available from: <http://robonaut.jsc.nasa.gov/hands.htm>, Accesed 2007-06-15
- Oxford University Gazette. Artificial Hand goes on trial . April 24th 1997, Accesed 2007-06-15



Human Robot Interaction

Edited by Nilanjan Sarkar

ISBN 978-3-902613-13-4

Hard cover, 522 pages

Publisher I-Tech Education and Publishing

Published online 01, September, 2007

Published in print edition September, 2007

Human-robot interaction research is diverse and covers a wide range of topics. All aspects of human factors and robotics are within the purview of HRI research so far as they provide insight into how to improve our understanding in developing effective tools, protocols, and systems to enhance HRI. For example, a significant research effort is being devoted to designing human-robot interface that makes it easier for the people to interact with robots. HRI is an extremely active research field where new and important work is being published at a fast pace. It is neither possible nor is it our intention to cover every important work in this important research field in one volume. However, we believe that HRI as a research field has matured enough to merit a compilation of the outstanding work in the field in the form of a book. This book, which presents outstanding work from the leading HRI researchers covering a wide spectrum of topics, is an effort to capture and present some of the important contributions in HRI in one volume. We hope that this book will benefit both experts and novice and provide a thorough understanding of the exciting field of HRI.

How to reference

In order to correctly reference this scholarly work, feel free to copy and paste the following:

Marcin Kaczmarek (2007). Human-Robot Interface for End Effectors, Human Robot Interaction, Nilanjan Sarkar (Ed.), ISBN: 978-3-902613-13-4, InTech, Available from:

http://www.intechopen.com/books/human_robot_interaction/human-robot_interface_for_end_effectors

INTECH
open science | open minds

InTech Europe

University Campus STeP Ri
Slavka Krautzeka 83/A
51000 Rijeka, Croatia
Phone: +385 (51) 770 447
Fax: +385 (51) 686 166
www.intechopen.com

InTech China

Unit 405, Office Block, Hotel Equatorial Shanghai
No.65, Yan An Road (West), Shanghai, 200040, China
中国上海市延安西路65号上海国际贵都大饭店办公楼405单元
Phone: +86-21-62489820
Fax: +86-21-62489821

© 2007 The Author(s). Licensee IntechOpen. This chapter is distributed under the terms of the [Creative Commons Attribution-NonCommercial-ShareAlike-3.0 License](https://creativecommons.org/licenses/by-nc-sa/3.0/), which permits use, distribution and reproduction for non-commercial purposes, provided the original is properly cited and derivative works building on this content are distributed under the same license.

IntechOpen

IntechOpen